Proceedings of the 2007 American Control Conference
Marriott Marquis Hotel at Times Square
New York City, USA, July 11-13, 2007

Simulation of Piezoelectric Tube Actuators by Reduced Finite Element Models for Controller Design

Johannes Maess, Andrew J. Fleming and Frank Allgöwer

Abstract— **This article presents an extended modeling approach for piezoelectric tube actuators combining Finite Element Analysis (FEA) and model order reduction (MOR) techniques. The model includes the full coupling between motion in all axes, while the reduced model order, which depends mainly on the desired bandwith and model accuracy, makes it a suitable basis for controller design purposes. Simulation results in the frequency domain are compared to measurements and show an excellent agreement in a wide frequency range. The increase of scan accuracy in closed-loop operation is demonstrated by simulation data of a model-based H_∞ controller.**

I. INTRODUCTION

Piezoelectric tube actuators are widely used in nanopositioning applications such as scanning tunneling microscopes [1], atomic force microscopes (AFM) [2] and nanofabrication [3]. They offer sub-nanometer resolution in all three translational degrees of freedom together with a compact design which is easy to implement in microscopes [4]. In AFM applications, the desired high-precision positioning capability of tube scanners is reduced by induced structural vibrations [4], dynamics-coupling caused errors [5], nonlinear hysteresis effects in relatively long-range scans [6] and drift caused by creep effects in slow operation modes [7]. Besides changes in the technical design of piezoelectric actuators [8], control theory has proven to be another possibility to overcome these performance limitations [9], [10].

The typical setup of a piezoelectric tube actuator is shown in Fig. 1. The lower end of the tube is clamped, while the upper one, denoted as tip, can freely move in all three dimensions. The outer surface of the tube is separated into quartered electrodes. The two pairs of opposite electrodes are used to generate a bending motion in either the x or y direction, which results in a lateral tip displacement along the respective axis. Two different configurations are distinguished: in the first one, only one of the two electrodes of a pair is voltage driven while the other is grounded (single electrode excitation); in the second, both electrodes of a pair are driven with equal but opposite voltages (twin electrode excitation) [4]. The lateral motion in the xy-plane is achieved by separately controlling the voltage input on the two electrode pairs. The inner surface of the tube is coated with an electrode, which is either grounded or voltage driven. A voltage applied to the inner electrode causes the tube to elongate, resulting in a z-axis displacement of the tube tip.

Due to the complexity of physical modeling [10], the linear vibrational dynamics of piezoscanners are often identified from experiments [9], [5], [11]. The focus of this paper is on the development of a piezoscanner model which accurately describes and predicts the linear structural dynamics up to high frequencies by simultaneously keeping the model order small enough for controller design and simulation purposes. By using the Finite Element Method for modeling piezoelectric structures [12], all coupling effects are included into the model. Furthermore, this approach offers high flexibility to model complicated geometries and all kinds of shapes of piezoelectric actuators. The model reduction procedure oriented towards the construction of a state-space model is based on modal reduction techniques and on observability and controllability considerations quantified by Hankel singular values [13]. Measurement data of frequency response functions and mode shapes is used for validation of the simulation model. The applicability of the low order model for feedback control is demonstrated by means of an H_∞ controller for improvement of tracking accuracy in closed-loop operation.

II. COUPLED FINITE ELEMENT MODEL

Modeling of piezoelectric devices with three-dimensional finite elements is applied nowadays to a wide variety of actuators and sensors, e.g. beam actuators [14] and smart structures [15]. Whereas existing 3D finite element models of piezoelectric tube scanners are restricted to calculation of static deformations [16], the present article extends this approach to the investigation of the tube scanner dynamics.

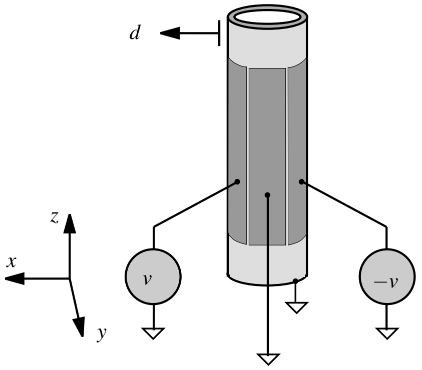

Fig. 1. A piezoelectric tube scanner developing a lateral tip displacement d as response to an anti-symmetric driving voltage v.

J. Maess and F. Allgöwer are with the Institute for Systems Theory and Automatic Control, University of Stuttgart, Pfaffenwaldring 9, 70550 Stuttgart, Germany (email: {maess, allgower}@ist.uni-stuttgart.de)

A. J. Fleming is with the School of Electrical Engineering and Computer Science, The University of Newcastle, Australia (email: andrew.fleming@newcastle.edu.au)

1-4244-0989-6/07/$25.00 ©2007 IEEE.

All dynamics-coupling effects between the scan axes are taken into account by considering the three-dimensional piezoelectric constitutive law

$$\begin{aligned} \mathbf{T} &= \mathbf{c}^{\mathrm{E}}\mathbf{S} - \mathbf{eE} \\ \mathbf{D} &= \mathbf{eS} + \varepsilon^{\mathrm{S}}\mathbf{E}, \end{aligned}$$

with mechanical stress matrix $\mathbf{T}$, mechanical strain matrix $\mathbf{S}$, electric field vector $\mathbf{E}$ and electric charge vector per unit area $\mathbf{D}$. The anisotropic material properties of the radially polarized piezoceramic are described by the mechanical stiffness matrix at constant electric field $\mathbf{c}^{\mathrm{E}}$, the permittivity matrix under constant strain ε^{S} and the piezoelectric stress matrix $\mathbf{e}$. After assembling the element matrices, the FE formulation of the equations of motion takes the general form

$$\mathbf{M}\ddot{\mathbf{x}} + \mathbf{C}\dot{\mathbf{x}} + \mathbf{K}\mathbf{x} = \mathbf{F} \tag{1}$$

with mass matrix $\mathbf{M}$, stiffness matrix $\mathbf{K}$ and external loads $\mathbf{F}$. Rayleigh damping is assumed for the finite element model via the damping matrix $\mathbf{C}$. The order of the fully coupled finite element model is denoted as n. Because of the coupling between structural and piezoelectric domains, the state vector $\mathbf{x}$ is composed of nodal displacements $\mathbf{u}$ and nodal electric potentials ϕ.

The FEA is applied to gain an overwiew and to allow predictions on the dynamics of piezoelectric tube scanners. A summary of the results of a sufficiently fine meshed modal analysis for the first 12 eigenmodes is presented in Tab. I. Specifically, a classification of mode shapes is possible by inspection of their 3D-represantations illustrated in Fig. 2. It is obvious that the first two eigenfrequencies correspond to longitudinal Bernoulli beam-type bending modes. For higher frequencies, other types of mode shapes, like circumferential shell bending modes, occur. All longitudinal and circumferential bending modes appear twice due to the axis-symmetric geometry of the tube. Fig. 2 concentrates on the mode shapes relevant for lateral scanner motion, therefore the torsional and elongational modes are omitted. From a control theory point of view, it is important to know that the circumferential bending modes appear at high frequencies and do not influence the operational deflection shapes in the low frequency range. Thus, it is sufficient to prevent the excitation of the first longitudinal bending mode to achieve the performance requirements for high accuracy scanning.

TABLE I

SUMMARY OF THE FULL FEM MODAL ANALYSIS.

No.	Freq. [kHz]	Mode Shape Classification
1,2	1.21	1st Longitudinal Bending
3,4	6.49	2nd Longitudinal Bending
5	6.97	Torsion
6	11.30	Elongation
7,8	13.98	1st Circumferential Bending
9,10	14.50	2nd Circumferential Bending
11,12	15.38	3rd Longitudinal Bending

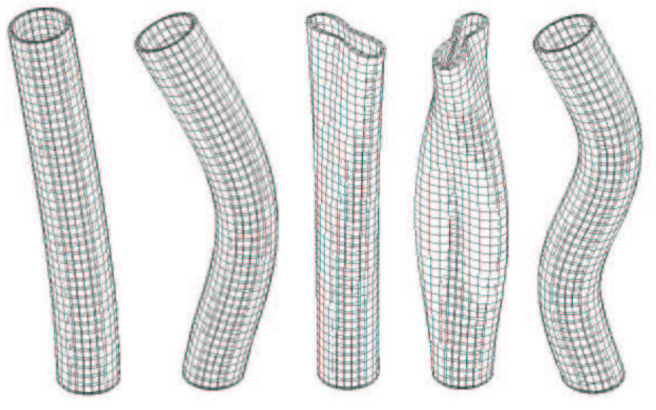

Fig. 2. 3D finite element mode shapes; from left to right: 1st longitudinal bending mode, 2nd longitudinal bending mode, 1st circumferential bending mode, 2nd circumferential bending mode, 3rd longitudinal bending mode.

III. LOW ORDER MODEL

The full finite element model of Eq. (1) is neither applicable to time domain simulations nor to controller design and implementation due to its high order n. For the model reduction process, the electrical potential degrees of freedom are partitioned into degrees of freedom on the grounded electrodes ϕ_{g}, on the potential electrodes ϕ_{p} and in the interior of the piezoelectric tube ϕ_{i} [17]. For the multi-input case, with two independently driven potential electrodes ϕ_{p_1} and ϕ_{p_2}, Eq. (1) is rewritten as

$$\begin{bmatrix} \mathbf{M}_{\mathrm{ss}} & \mathbf{0} & \mathbf{0} & \mathbf{0} & \mathbf{0} \\ \mathbf{0} & \mathbf{0} & \mathbf{0} & \mathbf{0} & \mathbf{0} \\ \mathbf{0} & \mathbf{0} & \mathbf{0} & \mathbf{0} & \mathbf{0} \\ \mathbf{0} & \mathbf{0} & \mathbf{0} & \mathbf{0} & \mathbf{0} \\ \mathbf{0} & \mathbf{0} & \mathbf{0} & \mathbf{0} & \mathbf{0} \end{bmatrix} \begin{bmatrix} \ddot{\mathbf{u}} \\ \ddot{\phi}_{\mathrm{i}} \\ \ddot{\phi}_{\mathrm{p}_1} \\ \ddot{\phi}_{\mathrm{p}_2} \\ \ddot{\phi}_{\mathrm{g}} \end{bmatrix} + \begin{bmatrix} \mathbf{K}_{\mathrm{ss}} & \mathbf{K}_{\mathrm{si}} & \mathbf{K}_{\mathrm{sp}_1} & \mathbf{K}_{\mathrm{sp}_2} & \mathbf{K}_{\mathrm{sg}} \\ \mathbf{K}_{\mathrm{si}}^{\mathrm{T}} & \mathbf{K}_{\mathrm{ii}} & \mathbf{K}_{\mathrm{ip}_1} & \mathbf{K}_{\mathrm{ip}_2} & \mathbf{K}_{\mathrm{ig}} \\ \mathbf{K}_{\mathrm{sp}_1}^{\mathrm{T}} & \mathbf{K}_{\mathrm{ip}_1}^{\mathrm{T}} & \mathbf{K}_{\mathrm{p}_1\mathrm{p}_1} & \mathbf{K}_{\mathrm{p}_1\mathrm{p}_2} & \mathbf{K}_{\mathrm{p}_1\mathrm{g}} \\ \mathbf{K}_{\mathrm{sp}_2}^{\mathrm{T}} & \mathbf{K}_{\mathrm{ip}_2}^{\mathrm{T}} & \mathbf{K}_{\mathrm{p}_1\mathrm{p}_2}^{\mathrm{T}} & \mathbf{K}_{\mathrm{p}_2\mathrm{p}_2} & \mathbf{K}_{\mathrm{p}_2\mathrm{g}} \\ \mathbf{K}_{\mathrm{sg}}^{\mathrm{T}} & \mathbf{K}_{\mathrm{ig}}^{\mathrm{T}} & \mathbf{K}_{\mathrm{p}_1\mathrm{g}}^{\mathrm{T}} & \mathbf{K}_{\mathrm{p}_2\mathrm{g}}^{\mathrm{T}} & \mathbf{K}_{\mathrm{gg}} \end{bmatrix} \begin{bmatrix} \mathbf{u} \\ \phi_{\mathrm{i}} \\ \phi_{\mathrm{p}_1} \\ \phi_{\mathrm{p}_2} \\ \phi_{\mathrm{g}} \end{bmatrix} = \begin{bmatrix} \mathbf{f} \\ \mathbf{q}_{\mathrm{i}} \\ \mathbf{q}_{\mathrm{p}_1} \\ \mathbf{q}_{\mathrm{p}_2} \\ \mathbf{q}_{\mathrm{g}} \end{bmatrix}$$

where damping is omitted for brevity of exposition. The electrical charges on the grounded electrodes, on the interior electrical degrees of freedom and on the two potential electrodes are denoted as $\mathbf{q}_{\mathrm{g}}, \mathbf{q}_{\mathrm{i}}$ and $\mathbf{q}_{\mathrm{p}_i}, i = 1,2$, respectively. There is no electrical potential associated with the grounded electrodes $\left(\phi_{\mathrm{g}} = 0\right)$; thus, the fifth line and fifth column in the mass and stiffness matrices are deleted. On each potential electrode, all nodes have the same potential, i.e. $\phi_{p_1,1} = \phi_{p_1,2} = \cdots = \phi_{p_1,j}$ for the j nodes on the first potential electrode. With a transformation matrix $\mathbf{T}_1$, which is typically chosen as a coincidence matrix, the nodal potential degrees of freedom ϕ_{p_1} on the first potential electrode are reduced to one potential master degree of freedom ϕ_{e_1} with the transformation law $\phi_{\mathrm{p}_1} = \mathbf{T}_1\phi_{\mathrm{e}_1}$. An analog transformation is performed for the second potential electrode. The input voltage of the scanner is applied to the master degrees of freedom on the potential electrodes ϕ_{e_1} and ϕ_{e_2}. Thus, by moving the excitation terms on the right side, one obtains the dynamic equations

$$\underbrace{\begin{bmatrix}\mathbf{M}_{\mathrm{ss}} & \mathbf{0}\\ \mathbf{0} & \mathbf{0}\end{bmatrix}}_{\mathbf{M}_{\mathrm{EV}}}\begin{bmatrix}\ddot{\mathbf{u}}\\ \ddot{\phi}_{\mathrm{i}}\end{bmatrix}+\underbrace{\begin{bmatrix}\mathbf{K}_{\mathrm{ss}} & \mathbf{K}_{\mathrm{si}}\\ \mathbf{K}_{\mathrm{si}}^{\mathrm{T}} & \mathbf{K}_{\mathrm{ii}}\end{bmatrix}}_{\mathbf{K}_{\mathrm{EV}}}\begin{bmatrix}\mathbf{u}\\ \phi_{\mathrm{i}}\end{bmatrix}= -\underbrace{\begin{bmatrix}\mathbf{K}_{\mathrm{sp}_1}\mathbf{T}_1 & \mathbf{K}_{\mathrm{sp}_2}\mathbf{T}_2\\ \mathbf{K}_{\mathrm{ip}_1}\mathbf{T}_1 & \mathbf{K}_{\mathrm{ip}_2}\mathbf{T}_2\end{bmatrix}}_{\mathbf{K}_{\mathrm{exc}}}\begin{bmatrix}\phi_{\mathrm{e}_1}\\ \phi_{\mathrm{e}_2}\end{bmatrix}, \tag{2}$$

where the external structural loads $\mathbf{f}$ and internal charges $\mathbf{q}_{\mathrm{i}}$ are assumed to be zero. For harmonic excitation $\phi_{\mathrm{e}_i} = \phi_{0_i}\mathrm{e}^{\mathrm{j}\omega_i t}, i = 1,2$, the corresponding eigenvalue problem is given by

$$\mathbf{K}_{\mathrm{EV}}\psi_r = \omega_r^2\mathbf{M}_{\mathrm{EV}}\psi_r \tag{3}$$

with the eigenvectors ψ_r. The eigenvalue problem is solved numerically for $m \ll n$ low-frequency mode shapes, which are collected in the modal matrix $\Psi \in \mathbb{R}^{n\times m}$. The modal matrix Ψ is the truncated basis for the transformation of the nodal displacements $\mathbf{u}$ into modal coordinates $\mathbf{q}$ with the transformation law $\mathbf{u} = \Psi\mathbf{q}$.

The modal mass and stiffness matrices are normalized to the identity matrix $\mathbf{I} \in \mathbb{R}^{m\times m}$ and the spectral matrix $\Lambda \in \mathbb{R}^{m\times m}$, respectively, by

$$\mathbf{M}_{\mathrm{m}} = \Psi^{\mathrm{T}}\mathbf{M}_{\mathrm{EV}}\Psi = \mathbf{I} \tag{4}$$

$$\mathbf{K}_{\mathrm{m}} = \Psi^{\mathrm{T}}\mathbf{K}_{\mathrm{EV}}\Psi = \Lambda = \mathrm{diag}\left(\omega_r^2\right) \tag{5}$$

where ω_r is the circular eigenfrequency of the rth eigenmode.

For the investigation of specific input-output behavior, the system order can be further reduced by selecting those mode shapes, which are dominant for the system in terms of controllability and observability considerations. To this end, the normal mode model from Eqs. (4) and (5) is transformed into the modal state-space representation

$$\begin{aligned}\dot{\mathbf{x}} &= \underbrace{\begin{bmatrix}\mathbf{0} & \mathbf{I}\\ -\Lambda & -\Gamma\end{bmatrix}}_{\mathbf{A}_{\mathrm{red}}}\mathbf{x}+\underbrace{\begin{bmatrix}\mathbf{0}\\ -\Psi^{\mathrm{T}}\mathbf{K}_{\mathrm{exc}}\end{bmatrix}}_{\mathbf{B}_{\mathrm{red}}}\mathbf{u}\\ \mathbf{y} &= \underbrace{\begin{bmatrix}\mathbf{c}\Psi & \mathbf{0}\end{bmatrix}}_{\mathbf{C}_{\mathrm{red}}}\mathbf{x}\end{aligned} \tag{6}$$

with the state space vector $\mathbf{x} = \left[\mathbf{q}^{\mathrm{T}}, \dot{\mathbf{q}}^{\mathrm{T}}\right]^{\mathrm{T}}$ and the input vector $\mathbf{u} = [\phi_{\mathrm{e}_1}, \phi_{\mathrm{e}_2}]^{\mathrm{T}}$. The matrix $\mathbf{c}$ is denoted as output shape matrix defining the desired degrees of freedom for the output y which is given in physical nodal quantities. On the one hand, the damping matrix Γ may represent Rayleigh damping using standard parameters of piezoelectric materials leading to adequate model accuracy for prediction of the dynamic behavior e.g. resulting from changes in geometrical properties without the need of system identification. On the other hand, Γ may be fitted to measurement results via modal damping parameters to further improve accuracy for model based controller design of specific configurations.

In structural dynamics, controllability of a mode can be used as a measure of its excitation by input actuation. Accordingly, the influence of the modal states on the system outputs is described by observability. The controllability and observability of the modes is quantified for linear systems by calculating the controllability Gramians $\mathbf{W}_{\mathrm{c}}$ and observability Gramians $\mathbf{W}_{\mathrm{o}}$. For systems in modal representation, the controllability and observability Gramians are diagonally dominant [13], i.e. $\mathbf{W}_{\mathrm{c}} \approx \mathrm{diag}(w_{\mathrm{c}i})$ and $\mathbf{W}_{\mathrm{o}} \approx \mathrm{diag}(w_{\mathrm{o}i})$, where $w_{\mathrm{c}i}$ and $w_{\mathrm{o}i}$ are the modal controllability and observability coefficients of the ith mode. For a SISO system, the transfer function of a modal state-space model is given as $G(s) = \mathbf{C}_{\mathrm{red}}(s\mathbf{I}-\mathbf{A}_{\mathrm{red}})^{-1}\mathbf{B}_{\mathrm{red}}$. Additionally, the structural transfer function is a composition of modal transfer functions G_{m_i} of the mode i, i.e. $G(\omega) = \sum_{i=1}^{n} G_{m_i}(\omega)$. The contribution of the jth mode to the SISO transfer function $G(\omega)$ can be quantified by the modal H_∞ norm $\parallel G_{m_j} \parallel_\infty = 2\gamma_j$, where γ_j denotes the Hankel singular value (HSV) of the jth mode with $\gamma_j = \sqrt{w_{\mathrm{c}j}w_{\mathrm{o}j}}$ for systems with low modal damping ratios [13]. Thus, modes with low HSVs and therefore low modal norms are deleted from the reduction basis Ψ of Eqs. (4) and (5), finally resulting in the transformation basis $\Psi_{\mathrm{HSV}} \in \mathbb{R}^{n\times m_{\mathrm{HSV}}}$.

IV. RESULTS AND DISCUSSION

In the frequency domain, simulation results are compared to measurement results for single electrode excitation as well as twin electrode excitation by means of frequency response functions (FRF) of the tip displacement d in the direction of excitation. The good agreement between measurement and simulation is supported by comparing the mode shapes of longitudinal bending modes.

A. Experimental Apparatus

As pictured in Fig. 3(a), the experimental apparatus comprises a piezoelectric tube glued into a recessed aluminum base, mounted onto an optical table. The tube was manufactured by Boston PiezoOptics from high-density PZT-5H piezoceramic. Four equally spaced silver electrodes are deposited in quadrature around the tube circumference. Relevant physical dimensions are described in Fig. 3(b).

The tip displacement frequency response and mode shapes were measured using a Polytec PI PSV300 laser doppler

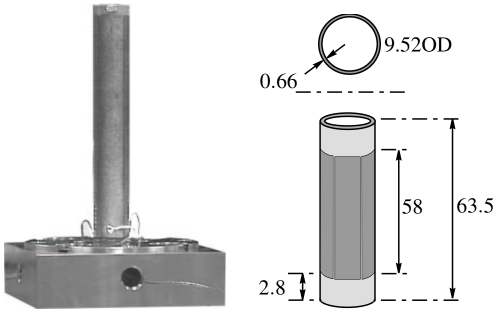

(a) Tube actuator glued into an aluminum base.

(b) Tube dimensions in mm.

Fig. 3. Measurement setup.

vibrometer. A 5.5 Volt periodic chirp was applied with a bandwidth of 20 kHz to either a single electrode, or anti-symmetrically to opposite electrodes. Periodic time histories were recorded at 52.1 kHz and used to compute a 6400 line FFT. Mode shapes were computed from 85 equally spaced complex frequency responses recorded vertically up the z-axis.

B. Single electrode excitation

In simulations, a 1 V sinusoidal input voltage is applied to one of the x-axes electrodes, while all the other electrodes are grounded. The output degree of freedom of the FRF is the x-displacement of the node on the tube tip located on the x-axes on the outer diameter. In the modeling process, this degree of freedom is selected via the output shape matrix $\mathbf{c}$. The single electrode excitation represents the SISO case, which is dominated by the HSVs of the first and second longitudinal bending modes. All longitudinal bending modes occur in a pair with the two eigenvectors normal to each other but arbitrarily oriented in the xy-plane. For SISO systems, with the input actuation and the considered output signal pointing into the same direction, it is always possible to rotate the eigenvectors such that one eigenvector of a pair is oriented along the input-output direction, such that the corresponding mode shape captures all the contributions to the system response. The influence of a static correction term in form of attachment modes is found to be negligible. Thus, a total of $m_{\text{HSV}} = 2$ mode shapes is included into the transformation basis Ψ_{HSV}.

Fig. 4 and Fig. 5 show a comparison of the FRFs of the measurement data, the simulated full finite element model with $2n = 31488$ states and the simulated reduced low order model with $2m_{HSV} = 4$ states. It is obvious from Fig. 4, that simulation and experiment agree very well for frequencies up to about 10 kHz. This frequency range includes the first two resonances of the system, which result from the excitation of the first two eigenfrequencies with longitudinal bending mode shapes. For the higher frequencies plotted in Fig. 5, simulation and measurement results diverge, which is due to the excitation of circumferential bending modes. These circumferential bending modes are difficult to measure; furthermore, damping of the high frequency modes might result in an overlap of two or more eigenmodes, such that the measured resonance corresponds to an operational deflection shape.

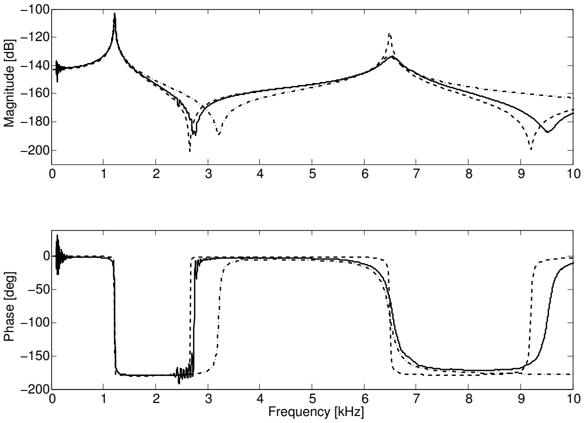

Fig. 4. Comparison of FRFs of measurement (solid curve), full finite element model (dashed curve), and reduced low order model (dashed-dotted curve) for single electrode excitation for low frequencies up to 10 kHz.

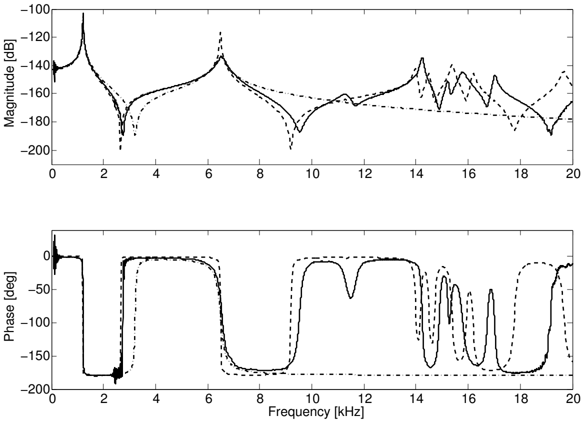

Fig. 5. Comparison of FRFs of measurement (solid curve), full finite element model (dashed curve), and reduced low order model (dashed-dotted curve) for single electrode excitation in the whole frequency range.

The first two eigenfrequencies of the simulation match the first two measured resonances with an error of less than 1%. The full finite element model shows some difference in the resonance amplitudes from the experimental data. It is thus concluded, that the Rayleigh damping, which is assumed for the full model, is not appropriate to precisely describe the damping effects in the whole frequency range. Therefore, a modal damping model with the diagonal damping matrix $\Gamma = \text{diag}(\Gamma_{rr})$ with $\Gamma_{rr} = 2\zeta_r\omega_r$ is incorporated into the low order model. The damping ratios ζ_r are determined from the measured FRFs by using an experimental modal analysis curve fitting tool. Fig. 4 confirms the excellent agreement of the resulting resonance amplitudes of the first two simulated eigenmodes. Furthermore, it can be seen that the model order reduction by means of HSV changes the zeros of the system whereas the poles of the reduced model are a subset of the poles of the full-order model.

The simulated and the experimentally determined mode shapes for selected eigenfrequencies are plotted in Fig. 6 in a 2D representation. The outputs are the x-displacements of points located on the outer diameter of the tube, centered in the middle of the potential electrode. The displacement at the tip of the tube ($z_{\text{rel}} = 1$) is scaled to unity for all mode shapes to make the simulation and measurement results comparable. For the first two mode shapes which belong to longitudinal bending modes, the simulation matches the experimental data very accurately. Furthermore, simulated and measurement data show a good agreement for the mode shape of the 3rd longitudinal bending mode.

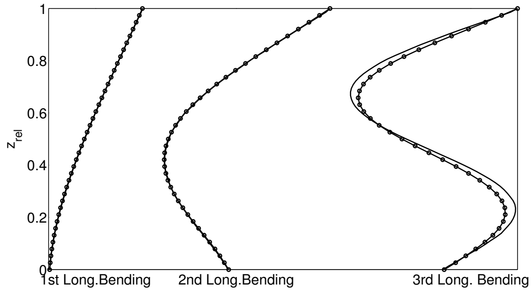

Fig. 6. Comparison of measured (solid curves) and simulated (dashed curves with marks) 2D mode shapes for single electrode excitation; from left to right: 1st longitudinal bending mode, 2nd longitudinal bending mode, 3rd longitudinal bending mode.

C. Twin electrode excitation

The twin electrode excitation is the simplest application of a multi-input situation to the system of the piezoelectric tube actuator. The reduction basis for the low order model is now composed of the first three longitudinal bending modes. The FRFs of measurement, full finite element model and reduced low order model are shown in Fig. 7. For the whole frequency range up to 20 kHz, the simulations match the measurement results quite accurately. This is due to the fact that for twin electrode configuration, the high-frequency circumferential bending modes are not excited. Because of their lateral symmetry, these modes are extinguished for the case of anti-symmetric excitation in the lateral plane. The resonance which is still apparent in Fig. 7 at approximately 15.4 kHz represents the third longitudinal bending mode. For this eigenmode, the eigenfrequency and resonance amplitude of the reduced low order model correspond satisfactorily to the measurement results. This supports the fact that the model represents very accurately the longitudinal bending of piezoelectric tube scanners up to high frequencies.

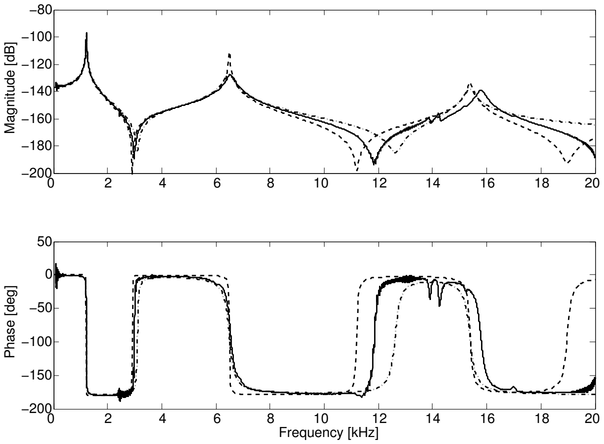

Fig. 7. Comparison of FRFs of measurement (solid curve), full finite element model (dashed curve), and reduced low order model (dashed-dotted curve) for twin electrode excitation.

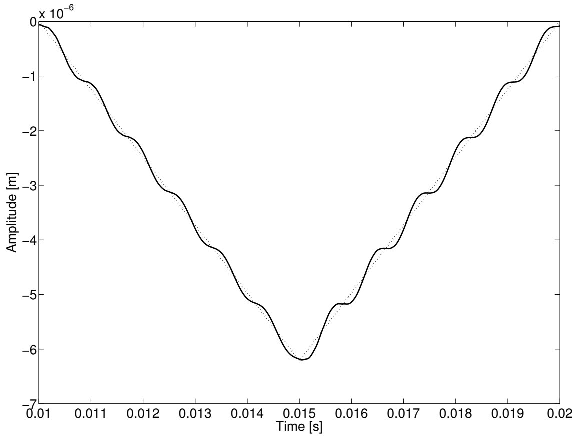

Fig. 8. Transient response of the tube tip to a 100 V amplitude, 100 Hz frequency triangular voltage input; solid curve: open loop, dotted curve: closed loop with H_∞ controller.

V. MODEL-BASED CONTROLLER DESIGN

The suitability of the low order model for controller design is demonstrated for the single electrode excitation setup. In typical AFM operation, the scan motion in the lateral xy-plane requires a triangular voltage input at one electrode pair, e.g. along the x-axis, while the other electrode pair for y-axis motion is driven with a stepwise increasing voltage input. In the first step towards control application described herein, the low order SISO model of Section IV-B with 4 states, which accounts for single electrode excitation and x-axis displacement as output, is considered for controller design.

In open loop operation, the triangle wave excitation as well as the square wave excitation for scan motion generation induce vibrations in the lateral dimensions of the tube which negatively affect the scan accuracy. The discontinuities of the triangular and stepwise voltage input excite the whole frequency spectrum of the piezolectric tube independent of the excitation frequency. Thus, the induced vibrations occur already at very low scan frequencies. For AFM operation, the triangular input voltage belongs to the fast scan axis and is considered in the following simulation data. The transient system response of the uncontrolled tube in Fig. 8 is distorted by induced vibrations, clearly dominated by the first longitudinal bending mode. This vibration is decaying very slowly due to the weak damping of the first resonance mode. In comparison, the higher damped second resonance is decaying much faster over time.

For the simulations, an H_∞ controller with a bandwith above the eigenfrequency of the second longitudinal eigenmode is calculated by means of a sensitivity weight synthesis problem. The controller of order 8 yields satisfactory robustness properties for closed-loop operation. The closed-loop bode diagram plotted in Fig. 9 shows that the resonance peaks in the system response are suppressed by the designed controller up to very high frequencies compared to the open-loop plant of Fig. 5. On the other hand, the anti-

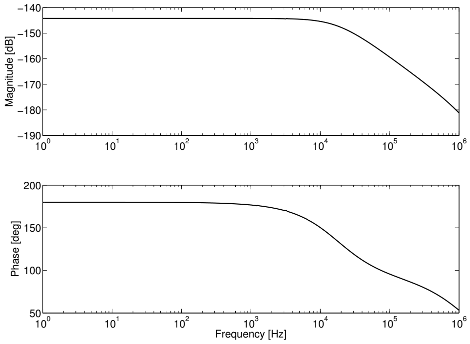

Fig. 9. Bode diagram of the closed-loop system with H_∞ controller.

resonances are also compensated by the controller, leading to an increase in the response at the corresponding frequencies. As demonstrated by the transient response for the closed-loop system in Fig. 8, the resonance vibrations are succesfully suppressed. The output displacement is very close to the desired triangular system response, indicating that the increased off-resonance amplitudes do not affect the performance of the closed-loop system. To account for higher-frequency content and test on controller robustness, the transient response of Fig. 8 is simulated with a reduced normal mode model with 40 states.

The described controller is so far not suited for implementation on typical AFM systems, since a measurement of the tip displacement, which is used as feedback signal for the controller design, is in general not possible. On the other hand, the good agreement of the model to the measured data allows the construction of a mixed feedforward-feedback controller, in which the presented controller might be used as the feedforward portion.

VI. CONCLUSIONS AND OUTLOOK

This paper presents a method to accurately model the dynamics of piezoelectric tube scanners while the system order is kept small for specific input-output configurations allowing transient simulations and controller design. The high quality of the model is validated by comparing selected dynamic simulation results to experimental data, showing in general a good agreement. The full order finite element model is primarily used for detailed prediction of the dynamic behavior even in the high frequency range. Compared to other modeling approaches, the method presented herein is the most complete for piezoelectric tube scanners in terms of linear dynamics, e.g. it automatically includes all coupling effects in dynamic operation. Furthermore, the finite element method offers high flexibility to account for further challenges in the modeling of piezoelectric tube scanners, for example the influence of the tip mass and sample holder including local radial stiffening effects; other collocations of electrodes in tube scanners, including an additional z-electrode on the outer surface; design imperfections like tube eccentricity as studied in [18] or tolerances in electrode placement and dimensions resulting in an asymmetric excitation with increased lateral coupling; and the modeling of other shapes of piezoelectric actuators and sensors like stack actuators or more complicated geometries. The described model reduction technique continues on this flexibility, enabling the investigation of all combinations of input-output situations of interest with moderate computational power. The overall modeling strategy always aims at a low order model such that model based control strategies can be applied to improve scan accuracy and increase scan speed in AFM operation.

REFERENCES

[1] G. Binning and D. P. E. Smith, "Single-tube three-dimensional scanner for scanning tunneling microscopy", *Rev. Sci. Instr.*, vol. 57, no.8, pp. 1688-1689, 1986.

[2] K. El Rifai, O. El Rifai, and K. Youcef-Toumi, "On dual actuation in atomic force microscopes", *in Proceedings of the American Control Conference*, Boston, Massachussets, pp. 3128-3133, 2004.

[3] D. Croft, D. McAllister, and S. Devasia, "High-speed scanning of piezo-probes for nano-fabrication", *Trans. ASME, J. Manufact. Sci. Technol.*, vol. 120, pp. 617-622,1998.

[4] A. J. Fleming and S. O. R. Moheimani, "Sensorless vibration suppression and scan compensation for piezoelectric tube nanopositioners", *IEEE Trans. Contr. Syst. Techn.*, vol. 14, no. 1, pp. 33-44, 2006.

[5] S. Tien, Q. Zou, and S. Devasia, "Iterative control of dynamics-coupling-caused errors in piezoscanners during high-speed AFM operation", *IEEE Trans. Contr. Syst. Techn.*, vol. 13, no. 6, pp. 921-931, 2005.

[6] M.-S. Tsai and J.-S. Chen, "Robust tracking control of a piezoactuator using a new approximate hysteresis model", *Trans. ASME, J. Dyn. Syst. Meas. Contr.*, vol. 125, pp.96-102, 2003.

[7] O. El Rifai and K. Youcef-Toumi, "Creep in piezoelectric scanners of atomic force microscopes", *in Proceedings of the American Control Conference*, Anchorage, Alaska, pp. 3777-3782, 2002.

[8] G. Schitter, K. J. Åström, B. DeMartini, G. E. Fantner, K. Turner, P. J. Thurner, and P. K. Hansma, "Design and modeling of a high-speed scanner for atomic force microscopy", *in Proceedings of the American Control Conference*, Minneapolis, Minnesota, pp. 502-507, 2006.

[9] D. Croft, G. Shed and S. Devasia, "Creep, hysteresis and vibration compensation for piezosctuators: Atomic force microscopy application", *Trans. ASME, J. Dyn. Syst. Meas. Contr.*, vol. 123, pp. 35-43, 2001.

[10] G. Schitter, P. Menold, H. F. Knapp, F. Allgöwer, and A. Stemmer, "High performance feedback for fast scanning atomic force microscopy", *Rev. Sci. Instr.*, vol. 72, no. 8, pp. 3320-3327, 2001.

[11] M. Ratnam, B. Bhikkaji, A. J. Fleming, and S. O. R. Moheimani, "PPF Control of a piezoelectric tube scanner", *in Proceedings of the 44th IEEE Conference on Decision and Control, and the European Control Conference*, Sevilla, Spain, pp. 1168-1173, 2005.

[12] U. Gabbert, T. N. Trajkov, and H. Köppe, "Modelling, control and simulation of piezoelectric smart structures using finite element method and optimal LQ control", *Facta Univers.*, vol. 3, no. 12, pp. 417-430, 2002.

[13] W. K. Gawronski, *Advanced Structural Dynamics and Active Control of Structures.* New York: Springer-Verlag, 2004.

[14] A. Benjeddou, M. A. Trindade, and R. Ohayon, "A unified beam finite element model for extension and shear piezoelectric actuators", *J. Intell. Mater. Syst. Struct.*, vol. 8, no. 12, pp. 1012-1025, 1997.

[15] Y.-H. Lim, "Finite-element simulation of closed loop vibration control of a smart plate under transient loading", *Smart Mater. Struct.*, vol. 12, pp. 272-286, 2003.

[16] R. G. Carr, "Finite element analysis of PZT tube scanner motion for scanning tunneling microscopy", *J. Micr.*, vol. 152, pp. 379-385, 1988.

[17] J. Becker, O. Fein, M. Maess, and L. Gaul, "Finite element-based analysis of shunted piezoelectric structures for vibration damping", *Computers & Structures*, accepted for publication.

[18] O. M. El Rifai and K. Youcef-Toumi, "Coupling in piezoelectric tube scanners used in scanning probe microscopes", *in Proceedings of the American Control Conference*, Arlington, Virginia, pp. 3251-3255, 2001.